

Real-Time Fault Detection and Accommodation for COTS Resolver Position Sensors

Douglas W. Brown, Derek L. Edwards, George Georgoulas, Bin B. Zhang, *Senior Member, IEEE*,
and George J. Vachtsevanos[‡], *Senior Member, IEEE*

Abstract— Resolver sensors are utilized as absolute position transducers to control the position and speed of actuators in many flight critical applications where robustness, accuracy and ability to operate in extreme environmental conditions are required. To ensure these requirements, several designs for self-diagnosing sensors were proposed in the past. However, such designs require additional instrumentation leading to further development and certification costs. To mitigate such costs, a methodology was sought to achieve similar self-diagnosis capabilities that can be retrofitted to already existing commercial off-the-shelf (COTS) resolver sensors. To achieve this goal, this paper proposes a new approach for real-time tracking of resolver faults with the ability to perform real-time fault detection. However, the additional benefit of this approach is the ability to accommodate faults in real-time once a fault is detected. The primary fault studied in this paper is resolver channel mismatch. A formulation based on the physical operating principles for a resolver sensor is provided. Diagnostic measures are identified for use in statistical-based fault-detection routines. Then, estimates for the resolver mismatch are tracked using a time-varying Kalman filter. Fault accommodation is achieved by applying the tracked estimates to adjust for the resolver mismatch. Finally, the fault detection and accommodation routines are evaluated in Simulink for an electro-mechanical actuator (EMA).

Index Terms— COTS, Fault Accommodation, Fault Diagnosis, Fault Tolerance, Physics of Failure, Sensors

I. INTRODUCTION

In recent years the use of electromechanical actuators in aerospace applications has increased thereby introducing brushless motor control systems into many flight critical applications. In these applications resolver sensors are preferred over similar transducers due to robustness, non-contacting working principle, measurement accuracy and resolution over a wide ambient temperature [1]. Therefore, it's essential in these safety critical applications that resolver faults be avoided at all costs. Several authors have previously presented and demonstrated designs for self-diagnosing resolver sensors. Sensor fault detection has traditionally been

achieved using hardware redundancy where three or more sensors are employed to measure the same quantity. The outputs of these sensors are monitored by a logic circuit which declares that a sensor is faulty if its signal deviates too far from the average value of the others [2]–[5]. Hardware redundant sensors can be replaced with virtual sensors to achieve analytical redundancy for sensor fault detection [6]. Virtual sensors are commonly used with a known system model to relate available measurements, i.e. speed and acceleration, with desired quantities such as position. Other designs rely on integrated fault detection circuitry in addition to the already existing sensor electronics [7]–[9]. However, such implementation leads to unnecessary costs due to further development time and certification. The alternative design discussed in this paper provides the ability to retrofit already existing COTS resolver sensors not only with real-time diagnosis but fault accommodation routines as well.

The remainder of this paper is organized as follows: Section II discusses the background of the resolver sensor and its related failure modes; Section III provides a formulation of the resolver fault model developed using first principles; Section IV presents simulation results for fault diagnosis and fault accommodation using the diagnostic indicators and estimation routines for an EMA system; And Section V summarizes the results concluded from this study.

II. BACKGROUND

Resolver sensors are utilized as absolute position transducers to control the position and speed of actuators in many industrial and aerospace applications. A resolver sensor consists of two components: a resolver and a RDC.

A. Resolver

Resolvers are rotary transformers consisting of one reference winding and two output windings. The reference winding is fixed on the stator [10]. An AC excitation signal, V_{ps} , with a frequency typically ranging from 1kHz – 10kHz is applied across the reference winding [11], [12]. The reference winding is magnetically coupled to both stator output windings through the windings located on the rotating shaft. A diagram illustrating the placement of the reference and output windings with respect to the shaft is provided below in Fig 1(a). The two output windings are placed in quadrature on the

[‡] G. J. Vachtsevanos is the corresponding author, phone: 404-894-6252; fax:404-894-4130; e-mail: gjv@ece.gatech.edu.

D. W. Brown, D. L. Edwards, G. Georgoulas and B. B. Zhang are with the Georgia Institute of Technology, Atlanta, GA, 30341.

G. J. Vachtsevanos is with the Georgia Institute of Technology and Impact Technologies, LLC.

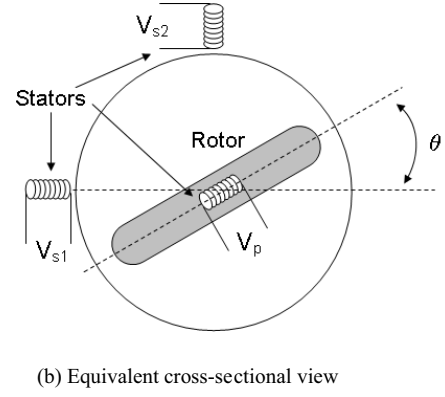
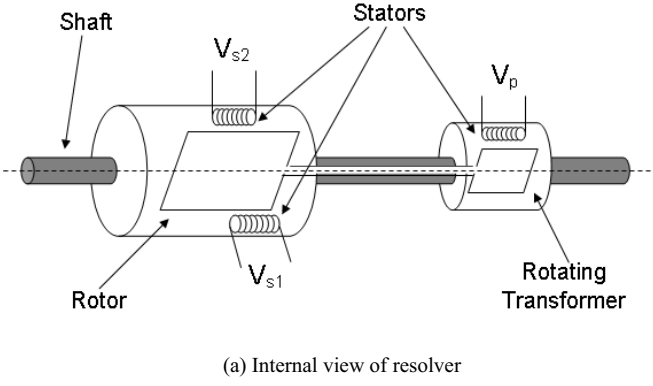


Fig 1. Diagram of a resolver transducer.

stator to generate two AC signals 90° out of phase [13]. Note, the voltages V_p , V_{s1} , and V_{s2} refer to the voltages applied to the reference winding and generated at the output windings accordingly. An *equivalent* cross-sectional view of the resolver is provided in Fig 1(b) illustrating the angular position of the rotor, θ , with respect to the windings.

When the rotor is at $\theta=0^\circ$, the voltage measured at V_{s1} and V_{s2} reaches a maximum and minimum respectively. If the rotor is further rotated in the positive direction, the voltage measured at V_{s1} and V_{s2} decreases and increases simultaneously until θ reaches 90° . Additional rotation in the positive direction will cause V_{s1} and V_{s2} to increase and decrease simultaneously until V_{s1} and V_{s2} reach a maximum and minimum again at 180° . A summary of equations governing this process is provided in (1) where f represents the carrier frequency of the reference signal. Note: the symbols V_o and K represent the amplitude of the input reference voltage V_p measured at the reference winding and the magnetic coupling coefficient (or ratio) between the reference and both output windings.

$$\begin{cases} V_p = V_o \sin(2\pi ft) \\ V_{s1} = (KV_o) \sin(2\pi ft) \cos(\theta) \\ V_{s2} = (KV_o) \sin(2\pi ft) \sin(\theta) \end{cases} \quad (1)$$

B. Resolver-to-Digital Converter (RDC)

The RDC is a commercially available integrated circuit (IC) used to compute the angular position from the resolver output

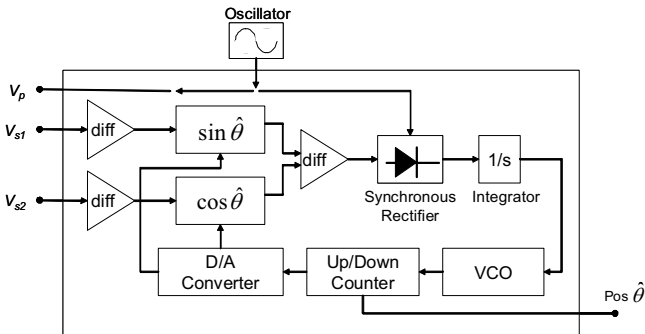


Fig 2. Resolver-to-digital converter block diagram.

signals V_{s1} and V_{s2} . A block diagram for a typical RDC is provided in Fig 2.

The RDC contains three inputs: an oscillator (or reference signal) and two measured signals V_{s1} and V_{s2} . The RDC also consists of two outputs, the recovered position angle $\hat{\theta}$ and the reference voltage V_p . The recovered position angle is calculated by multiplying V_{s1} and V_{s2} with $\sin \hat{\theta}$ and $\cos \hat{\theta}$ respectively [14]. Then, the difference of the resulting signals is computed using a difference amplifier. The resulting signal is expressed in (2).

$$V_d = V_{s1} \sin(\hat{\theta}) - V_{s2} \cos(\hat{\theta}) \quad (2)$$

The expression given in (2) can be simplified by first substituting the expressions for V_{s1} and V_{s2} provided in (1) and expanding the result,

$$V_d = KV_o \sin(2\pi ft) [\cos(\theta) \sin(\hat{\theta}) - \sin(\theta) \cos(\hat{\theta})]. \quad (3)$$

Next, a trigonometric identity for the difference of two angles further simplifies (3) to,

$$V_d = KV_o \sin(2\pi ft) \sin(\hat{\theta} - \theta). \quad (4)$$

Finally, a synchronous rectifier and integrator are used to remove the carrier frequency from V_d . The resulting RMS signal is fed into a voltage controlled oscillator (VCO). The VCO generates a clock signal proportional to the RMS signal which drives a digital up/down counter [14]. The up-down counter is used to generate a digital value for $\hat{\theta}$. A digital-to-analog converter is used to update the input signal multipliers ($\sin \hat{\theta}$ and $\cos \hat{\theta}$) discussed earlier. The counter reaches steady-state when the root-mean-squared (RMS) value of V_d approaches zero thereby allowing $\hat{\theta}$ to approach θ .

C. Failure Modes

Resolver faults can be classified under four categories: (1) resolver winding faults such as opens or shorts, (2) interconnection faults, (3) ancillary component faults and (4)

TABLE I
FMECA FOR BRUSHLESS MOTOR / RESOLVER ASSEMBLY

| Item / Component | Failure Rate (hr ⁻¹) | Failure Mode / Cause |
|------------------------|----------------------------------|--|
| <i>Bearings</i> | 1.78E-05 | Increased friction due to - bearing wear - galling. |
| <i>Position Sensor</i> | 1.70E-05 | Loss/incorrect feedback signal from resolver due to insulation faults: - Shorting between windings - Winding "open" - Winding "short" to ground |
| <i>Brushless Motor</i> | 1.03E-05 | Breakdown of stator assembly insulation due to: - Shorting between windings - Winding "open" - Winding "short" to ground |
| <i>Power Connector</i> | 6.64E-07 | Electrical open due to: - Open pin - Open leadwire |

resolver and a resolver-to-digital converter (RDC) faults such as internal circuit failure [7]. Table I provides results from an internal Failure Modes and Effects Analysis (FMECA) study of a brushless motor with a resolver sensor. Note, in this study emphasis was placed on the motor / resolver assembly thereby omitting the failure rates of the power electronics. Refer to [15] for additional information regarding a FMECA study for EMA electronic components.

D. Failure Effects

According to the FMECA study, most resolver related failure modes result from insulation faults primarily caused by shorting between windings, open circuits and short circuits. Effects from these failure modes result in attenuation of V_{s1} and/or V_{s2} [7]–[9] depending on the fault location. An insulation fault located at the reference winding results in a reduction in both V_{s1} and V_{s2} . Alternatively, a fault located at either output winding results in a reduction in either V_{s1} or V_{s2} . Corresponding effects on V_{s1} or V_{s2} are illustrated in Fig 3.

Insulation faults located at the output winding result in an relative amplitude mismatch, or channel mismatch, between the signals V_{s1} and V_{s2} . This is critical since the RDC requires both signals to be matched to resolve the correct position. Note, this mismatch does not occur if the fault is located at the reference winding. Therefore, the remaining discussion regarding resolver faults will be respect to channel mismatch.

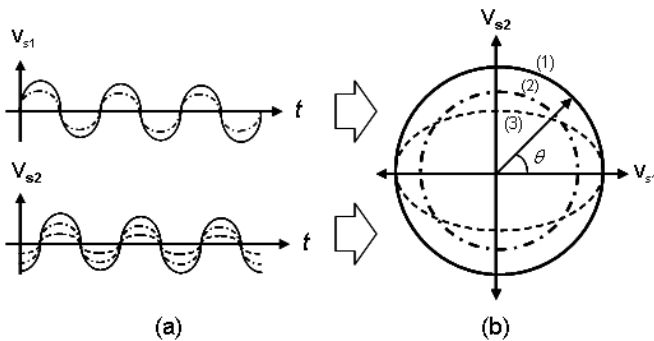


Fig 3. Resolver output signals plotted in (a) time domain and (b) phase domain for (1) no fault (2) insulation fault located at resolver reference and (3) insulation fault located at one of the resolver outputs.

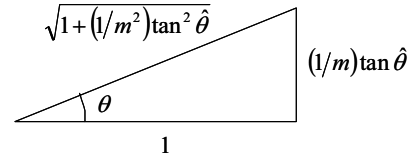


Fig 4. Trigonometric identify.

III. THEORY

This section outlines the development of a fault model from first principles to formulate a methodology to estimate channel mismatch and its associated uncertainties.

A. Fault Model

Small channel mismatches in the RDC result in a differential phase shift leading to position error. Channel mismatches can be characterized using the mismatch ratio m . The differential phase shift results when the RDC tracking loop, shown in Fig 2, forces (5) to zero when m is not-equal to unity.

$$m \sin(\theta) \cos(\hat{\theta}) - \cos(\theta) \sin(\hat{\theta}) \equiv 0 \Rightarrow \begin{cases} \theta = \hat{\theta} & \text{if } m = 1 \\ \theta \neq \hat{\theta} & \text{if } m < 1 \end{cases} \quad (5)$$

During normal conditions, when m is equal to unity, the tracking angle $\hat{\theta}$ approaches the actual resolver position θ . However, when m deviates from unity, either by increasing or decreasing from its nominal value, the tracking angle $\hat{\theta}$ corresponding to θ changes with the phase of θ as expressed in (6).

$$\hat{\theta} = \arctan(m \tan(\theta)). \quad (6)$$

This results in a differential phase mismatch $\Delta \hat{\theta}$ defined by,

$$\Delta \hat{\theta} = \hat{\theta} - \theta. \quad (7)$$

Applying the tangent function to both sides of (6) gives an implicit expression relating θ and $\hat{\theta}$ as shown in (8).

$$\tan(\hat{\theta}) = m \tan(\theta) \quad (8)$$

This relationship can also be viewed trigonometrically as illustrated in Fig 4. Taking the derivative of (8) implicitly produces the following relationship between the measured speed, $\tilde{\omega}$, and actual speed, ω ,

$$\left[\frac{1}{m} \sec^2(\hat{\theta}) \right] \tilde{\omega} = \left[\sec^2(\theta) \right] \omega \quad (9)$$

The secant-squared term for the rotor position θ in (9) can be expressed explicitly as a function of the tracking angle $\hat{\theta}$ by using the trigonometric relationship provided in Fig 4. The resulting expression simplifies to,

$$\frac{1}{m} \sec^2(\hat{\theta}) \tilde{\omega} = \left[1 + \frac{1}{m^2} \tan^2(\hat{\theta}) \right] \omega \quad (10)$$

Finally, let $r(t)$ be defined as the ratio of measured speed to actual speed,

$$r(t) \stackrel{\text{def}}{=} \tilde{\omega}(t)/\omega(t). \quad (11)$$

Using this definition, the expression given in (10) can be rewritten as a function entirely of $\hat{\theta}$,

$$m^2 - [r(t)\sec^2(\hat{\theta})]m + \tan^2(\hat{\theta}) = 0 \quad \text{where } r(t) > 0. \quad (12)$$

By applying the quadratic formula an explicit solution for m can be obtained,

$$m = \frac{1}{2} \left[r(t)\sec^2(\hat{\theta}) \pm \sqrt{r^2(t)\sec^4(\hat{\theta}) - 4\tan^2(\hat{\theta})} \right]. \quad (13)$$

By applying the appropriate trigonometric identities, the expression can be reduced to the simplified form,

$$m = \frac{[r(t) \pm \sqrt{r^2(t) - \sin^2(2\hat{\theta})}]}{2\cos^2(\hat{\theta})}, \quad (14)$$

which can be re-expressed as,

$$m = \frac{[r(t) \pm \sqrt{2r^2(t) - 1 + \cos(4\hat{\theta})}]/2}{1 + \cos(2\hat{\theta})}. \quad (15)$$

Note, it can be shown by taking the limit as $\hat{\theta}$ approaches periodic integer values of π the mismatch parameter, m , converges to,

$$\lim_{\hat{\theta}=k\pi} m = r(t) \quad \text{for } k \in \mathbb{Z}. \quad (16)$$

For small deviations in $\hat{\theta}$, corresponding deviation in the mismatch parameter, Δm , can be expressed as,

$$\Delta m \leq |r(t)| \left(\left| \frac{\Delta \tilde{\omega}}{\tilde{\omega}} \right| + \left| \frac{\Delta \hat{\omega}}{\hat{\omega}} \right| \right) \quad (17)$$

when $\hat{\theta} = k\pi$ for $k \in \mathbb{Z}$.

If measurements of $\hat{\theta}$ are restricted to the set,

$$S = \{ \hat{\theta} \in (k\pi - \varepsilon, k\pi + \varepsilon) \mid k \in \mathbb{Z} \}, \quad (18)$$

for sufficiently small values of $\varepsilon \ll 1$, then m and Δm can be estimated using point estimates of the mismatch parameter \hat{m} and its corresponding standard-deviation $\hat{\sigma}_m$ computed as,

$$\hat{m} = \frac{\tilde{\omega}(t)}{\hat{\omega}(t)}, \quad \hat{\sigma}_m \leq \frac{|\tilde{\omega}(t)|}{|\hat{\omega}(t)|} \cdot \left(\left| \frac{\Delta \tilde{\omega}}{\tilde{\omega}} \right| + \left| \frac{\Delta \hat{\omega}}{\hat{\omega}} \right| \right). \quad (19)$$

where $\hat{\omega}$ and $\Delta \hat{\omega}$ correspond to the estimated rotor speed and corresponding error derived from measurements of $\hat{\theta}$.

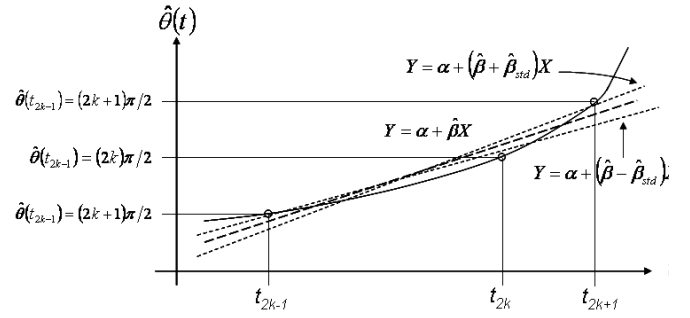


Fig 5. Geometric representation of $\hat{\beta}$ and $\hat{\beta}_{std}$

B. Feature Extraction

Assume the speed of the rotor is moving *sufficiently fast* such that the acceleration of the rotor is approximately constant and all corresponding time measurements, t_k , satisfy (20).

$$t_k = \left(t \in \mathbb{R}^+ \text{ s.t. } 0 \leq |\hat{\theta}(t) - \pi k/2| < \varepsilon \ll 1 \text{ for } k \in \mathbb{Z} \right) \quad (20)$$

where $r(t) > 0$

Then point estimates for $\hat{\omega}$ and $\Delta \hat{\omega}$ can be found at time t_{2k} by fitting the vector measurements, consisting of three consecutive time-correlated single-point measurements, $X(t_{2k}) = \{t_{2k-1}, t_{2k}, t_{2k+1}\}$ and $Y(t_{2k}) = \{\hat{\theta}(t_{2k-1}), \hat{\theta}(t_{2k}), \hat{\theta}(t_{2k+1})\}$ to the normal error linear regression model,

$$Y = \alpha + \beta X + \varepsilon, \quad (21)$$

where α and β are regression parameters, X and Y are sample vector measurements and ε_i is a zero-mean normally distributed random error term. The least-squares fit estimate for the regression parameter β and its associated standard deviation β_{std} can be found using the following formulas [16],

$$\hat{\beta} = \frac{\sum_{i=1}^3 (X_i - \bar{X})(Y_i - \bar{Y})}{\sum_{i=1}^3 (X_i - \bar{X})^2} \quad (22)$$

$$\hat{\beta}_{std} = \sqrt{\frac{1}{2} \left[\frac{\sum_{i=1}^3 \{Y_i - [\bar{Y} + \beta(X_i - \bar{X})]\}^2}{\sum_{i=1}^3 (X_i - \bar{X})^2} \right]} \quad (23)$$

Finally, using $\hat{\beta}$ and $\hat{\beta}_{std}$, point estimates for \hat{m} and $\hat{\sigma}_m$ can be re-expressed as,

$$\begin{cases} \hat{m}(t_{2k}) = \frac{\tilde{\omega}(t_{2k})}{\hat{\beta}(t_{2k})} \\ \hat{\sigma}_m(t_{2k}) \leq \frac{|\tilde{\omega}(t)|}{|\hat{\beta}(t_{2k})|} \cdot \left(\left| \frac{\Delta \tilde{\omega}}{\tilde{\omega}} \right| + \left| \frac{\hat{\beta}_{std}(t_{2k})}{\hat{\beta}(t_{2k})} \right| \right) \end{cases} \quad (24)$$

A geometric representation of the linear regression estimation of $\hat{\beta}$ and $\hat{\beta}_{std}$ is provided in Fig 5.

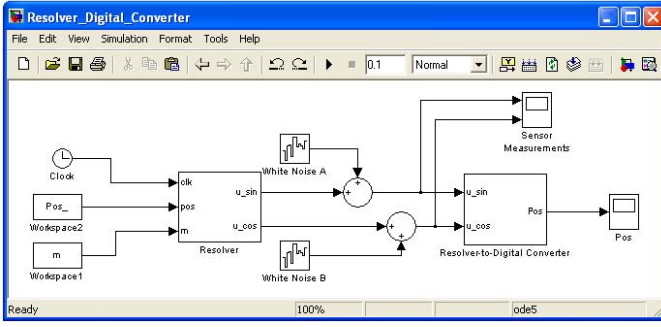


Fig 6. Simulink resolver fault model.

IV. SIMULATION

The fault model discussed earlier was evaluated in Simulink as shown in Fig 6. Models of the resolver and RDC were constructed using the mathematical representations presented earlier. Noise was added to the simulated sensor measurements to generate data representative of the real system [12].

The model was evaluated for an artificially generated fault profile for the mismatch parameter m . The resulting estimate of m along with an estimate of its associated standard deviation σ_m and position error are provided in Fig 7. Note, as the mismatch parameter m deviates from unity, the position error increases as well as the estimated values for the standard deviation.

A. Fault Detection

Hypothesis based testing using the z-test, depicted in Fig 8, was performed on the estimates of m to identify the occurrence of a fault. Gaussian distributions were used with the type I and type II errors both set to 0.05. A fault was declared when both errors were below the specified threshold.

B. Parameter Estimation

Assuming the mismatch parameter is slowly changing with degradation, a discrete time-varying Kalman filter can be used to estimate m [17]. Since only one state variable is necessary, the Kalman filter state equations reduce to the following [17],

$$\begin{cases} x(n+1) = x(n) + w(n) \\ y(n) = x(n) + v(n) \end{cases} \quad (25)$$

where w and v are represented using zero-mean Gaussian noise. The process noise, w , is modeled using a constant variance σ_w^2 . The standard deviation of the process noise may be estimated from (17) where the unknown quantities can be obtained from specifications provided by the manufacturer's datasheets. Whereas, the variance of the measurement noise, v , is modeled using a time-varying estimate, $\sigma_v^2(n)$. The standard deviation of the measurement noise can be estimated from (24) by using time varying estimated values of $\sigma_m(n)$ for each time instant. The Kalman filter estimate for m using the fault profile given earlier is shown in Fig 9. The intermittent region refers to the period of time between the occurrence of an incipient fault and fault detection.

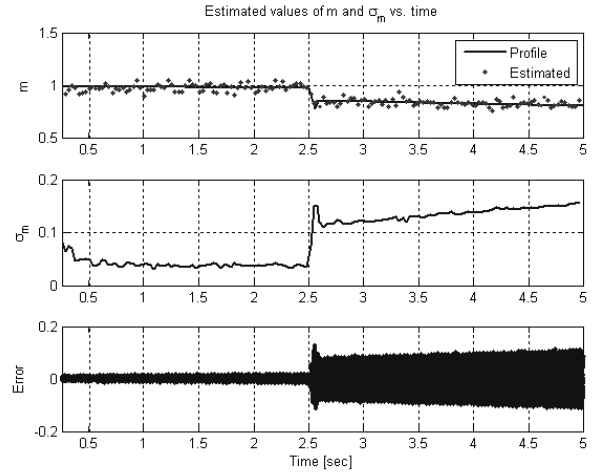


Fig 7. Simulation of resolver fault with estimates for m , σ_m and position error.

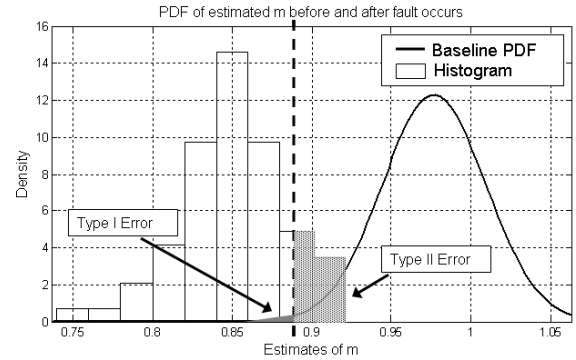


Fig 8. Illustration of Hypothesis testing for fault detection.

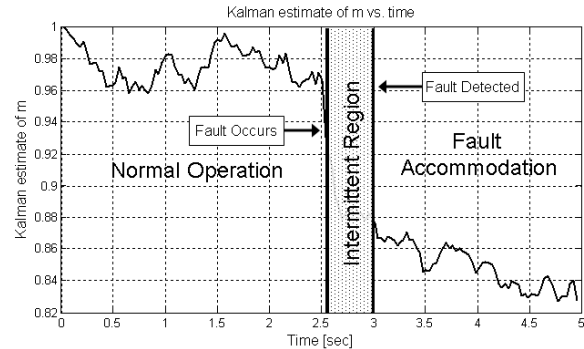


Fig 9. Kalman filter estimate of m vs. time for different health-state regions.

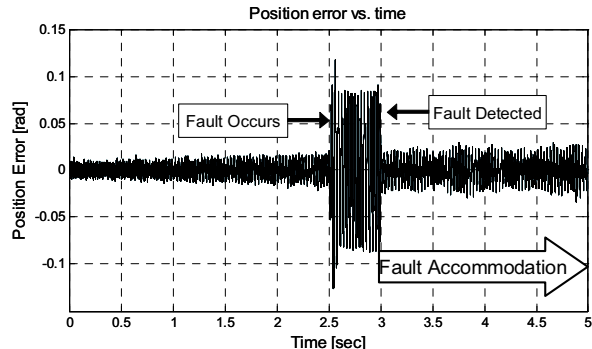


Fig 10. Position error vs. time with fault compensation after fault detection.

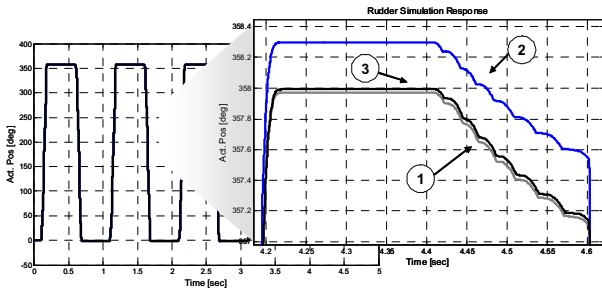


Fig 11. EMA Simulation for a (1) fault free case (2) fault case and (3) fault case with accommodation.

C. Fault Accommodation

After fault diagnosis, accommodation is performed using Kalman filter estimates of m to compensate for the channel mismatch using the following formula,

$$\Delta \hat{\theta}_{est}(\hat{\theta}) = \hat{\theta} - \arctan(\hat{m} \tan(\hat{\theta})), \quad (26)$$

where $\Delta \hat{\theta}_{est}$ represents the estimated differential phase shift corresponding to measurements of $\hat{\theta}$. The corresponding position error for the resolver sensor during a fault case with accommodation is provided in Fig 10. Notice, the position error increases after the occurrence of the incipient fault. However, once the fault is detected, the Kalman filter estimates are used to compensate for the channel mismatch using (26) thereby reducing the overall position error.

D. Performance Evaluation

The fault detection and accommodation routines were evaluated in Simulink for an electro-mechanical actuator (EMA). A pulse train command was applied to the input of the actuator. The expected, or ideal, actuator response is shown in Fig 11. Also provided is an expanded view of the fault free, fault case, and fault case with accommodation. The applied fault increased the steady-state error by 20%. However, applying fault accommodation routines after fault detection reduced the effects of the error introduced by the fault by approximately 90%.

V. CONCLUSION

A new design for a real-time fault detection and accommodation routine for a resolver position sensor was proposed. Unlike previous designs, the proposed design can be applied to already existing COTS sensors with no internal hardware modifications or additional sensors. The fault detection and accommodation routines rely on parameter estimation of resolver channel mismatch. A mathematical model representing channel mismatch was used with a physical model of the resolver and RDC to derive an algorithm to estimate channel mismatch. Finally, fault detection and accommodation routines identified in this paper were evaluated using a Simulink model of an EMA. The results demonstrated the merit of the approach. However, further validation is required using a hardware in the loop test-bench.

REFERENCES

- [1] G. Brasseur, "A Robust Capacitive Angular Position Sensor," *IEEE Instrumentation and Measurement Technology Conference*, June 4-6, 1996.
- [2] R. Isermann, R. Ulrich., "Intelligent Actuators - Ways to autonomous 1989 actuating systems," *Automatica*, vol. 29, No 5. pp. 1315-1331, 1993.
- [3] A. S. Victor, A. Joseph, J. D. John, "On line diagnosis of a self contained flight actuator," *IEEE Transactions on Aerospace and Electronic Systems*, vol. 30, no. 1, pp. 1315-1331, 1993
- [4] T. Pfeufer, "Application of model based fault detection and diagnosis to the quality assurance of an automotive actuator," *Control Eng Practice*, vol. 5, no. 5, pp 703-708, 1994.
- [5] S. B. Carl and S. Paul, "A model based approach to prognostics and health management for flight control actuators," *IEEE Aerospace Conference Proceedings*, pp 3551-3562, 2004.
- [6] M. Jayakumar and B. B. Das, "Fault Detection, Isolation and Reconfiguration in Presence of Incipient Sensor Faults in an Electromechanical Flight Control Actuation System," *IEEE International Conference on Industrial Technology*, pp 92-97, Dec 2006.
- [7] A. Murray, H. Bruce and A. Hirao, "Resolver Position Sensing System with Integrated Fault Detection for Automotive Applications," *Proc. of IEEE Sensors*, vol. 2, pp. 864 – 869, 2002.
- [8] M. Kobayashi and T Miya, *Resolver, resolver fault detection circuit, and resolver fault detection method*, US patent 6,803,781, to Minebea Co., Patent and Trademark Office, 2004.
- [9] A. Clark, K. Cook, R. D. Wittenbach and D. M. Kamath, *Method and apparatus for detecting faults in a resolver*, US patent 6,205,009, to Minebea Co., Patent and Trademark Office, 2001.
- [10] "56F80x Resolver Driver and Hardware Interface," AN1942, Application Note, Freescale Semiconductor, Chandler, Arizona, 2005.
- [11] M. Konghirum, "A Resolver-based Vector Control Drive of Permanent Magnet Synchronous Motor on a Fixed-Point Digital Signal Processor," *IEEE TENCN 2004*, November 21-24, 2004, Lotus Hotel Pang Suan Kaew, Chiangmai, Thailand, pp. 167-170.
- [12] "Variable Resolution Resolver-to-Digital Converter," AD2S83 Data Sheet, Analog Devices, Norwood, MA, 2000.
- [13] R. Hoseinnezhad, A. Bab-Hadiashar and P. Harding, "Calibration of Resolver Sensors in Electromechanical Braking Systems: A Modified Recursive Weighted Least-Squares Approach," *Trans. on Industrial Electronics*, vol. 54, no. 2, pp. 1052-1060, Apr. 2007.
- [14] "E-learning Resources in Microelectronics: Resolver," University of Paderborn. [Online]. Available: <http://data.bolton.ac.uk/mind/paderborn/sensors/resolver/resolver.html> [Accessed: May 19, 2008].
- [15] M. Baybutt, S. Nanduri, P. W. Kalgren, D. S. Bodden, N. S. Clements and S. Alipour, "Seeded Fault Testing and In-situ Analysis of Critical Electronic Components in EMA Power Circuitry," *IEEE Aerospace Conference*, 1-8 March 2008.
- [16] C. J. Nachtshiem, J. Neter, M. H. Kutner and W. Wasserman, *Applied Linear Statistical Models*, 5th Edition, McGraw-Hill, 2005.
- [17] M. H. Hayes, *Statistical Digital Signal Processing and Modeling*, John Wiley & Sons, New York, NY, USA, 1996.